

A Fourth Order Tensor Statistical Model for Diffusion Weighted MRI Application to Population Comparison

Theodosios Gkamas¹, Félix Renard², Christian Heinrich¹ and Stéphane Kremer¹

¹*ICube UMR 7357, University of Strasbourg – CNRS, Fédération de Médecine Translationnelle de Strasbourg (FMTS),
300 bd Sébastien Brant – CS 10413, 67412 Illkirch cedex, France*

²*Gipsa-lab, 11 rue des Mathématiques, Grenoble Campus BP 46, 38402 St Martin d'Hères cedex, France*

Keywords: Diffusion-weighted MRI, Fourth Order Tensor, Non Euclidean Metric, Nonlinear Dimension Reduction, Permutation Testing.

Abstract: In this communication, we propose an original statistical model for diffusion-weighted magnetic resonance imaging, in order to determine new biomarkers. Second order tensor (T2) modeling of Orientation Distribution Functions (ODFs) is popular and has benefited of specific statistical models, incorporating appropriate metrics. Nevertheless, the shortcomings of T2s, for example for the modeling of crossing fibers, are well identified. We consider here fourth order tensor (T4) models for ODFs, thus alleviating the T2 shortcomings. We propose an original metric in the T4 parameter space. This metric is incorporated in a nonlinear dimension reduction procedure. In the resulting reduced space, we represent the probability density of the two populations, normal and abnormal, by kernel density estimation with a Gaussian kernel, and propose a permutation test for the comparison of the two populations. Application of the proposed model on synthetic and real data is achieved. The relevance of the approach is shown.

1 INTRODUCTION

Diffusion-Weighted Magnetic Resonance Imaging (DW-MRI) is a unique way to probe the diffusion of water molecules in the human brain *in vivo*. The corresponding data provide information about the underlying white matter fiber tracts. Diseases such as multiple sclerosis, Alzheimer's disease, and stroke can be monitored using DW-MRI (Horsfield and Jones, 2002).

Data stemming from DW-MRI require mathematical modeling. Diffusion Tensor Imaging (DTI) is a popular description tool for such data (Jones, 2011). The Orientation Distribution Function (ODF) of a given voxel in white matter is accounted for by a six parameter model, also known as second order tensor (T2) model. The major limitation of the T2 model is its inability to account for crossing fibers. Nevertheless, accounting for crossing fibers is important since about half of the brain voxels are hosting crossings. To this end, the T2 ODF model has been generalized to a fourth order tensor (T4) model, comprising 15 parameters. This model encapsulates the T2 model as a particular case, and is able to account for fiber crossings (Weldeselassie et al., 2012). This versatility has led us to rely on T4 modeling (Ozarslan and Mareci,

2003; Weldeselassie et al., 2012; Tuch, 2004).

The goal of the present study is to propose an original statistical model related to T4 parameterization, in order to provide more efficient diagnosis and follow up tools for pathologies of interest. In particular, we aim at early diagnosis and at the determination of new biomarkers. Many statistical description models have been devised in the T2 framework (see *e.g.* (Arsigny et al., 2006)). The main concern is to account for the particular geometry of the underlying space in order to propose powerful tools. A popular model is the log-Euclidean one (Arsigny et al., 2006). The contribution of the present work is to propose a dedicated metric and corresponding statistics in the T4 framework.

A T4 ODF is parameterized by a vector in \mathbb{R}^{15} . This working space will be equipped with a suited metric. Besides, a 15-dimension space will be sparsely filled with data: for a given voxel of interest, we have a number of points corresponding to the number of patients (abnormal data) and controls (normal data), which is orders of magnitude below the number of points required to fill \mathbb{R}^{15} . Reduction of dimension of this space will improve the robustness of the subsequent statistical tests. We resort to a nonlinear dimension reduction procedure (Isomap (Tenenbaum

et al., 2000)) which is now widely used. Isomap has already been used for group comparison with classical statistical tests in the T2 framework (Verma et al., 2007). In the reduced space (the space of features), we propose here an original statistical discriminative test between the two populations. This test allows to detect the voxels of interest, permitting the discrimination between normal and abnormal and discovering voxels where the populations are significantly different (*i.e.* biomarker).

This communication is organized as follows. The proposed model is presented in section 2. We detail in particular the choice of the metric, the reduction of dimension, and the statistical test in the reduced space. Experimental results on synthetic data and on real data are shown in section 3. Conclusion is drawn in section 4.

2 PROPOSED STATISTICAL MODEL

This section presents the considered data parameterization, the chosen data normalization procedure, and the proposed statistical model.

2.1 T4 ODF Parameterization

A second order semi-definite Cartesian tensor writes $f(\mathbf{g}) = \mathbf{g}^T \mathbf{D} \mathbf{g}$, where \mathbf{g} is a unit vector of \mathbb{R}^3 corresponding to a given direction in space and \mathbf{D} is a matrix containing the coefficients of the tensor. Such a model may be used to represent ODFs (T2 ODF model).

The generalization to fourth order semi-definite Cartesian tensors writes:

$$f(\mathbf{g}) = \sum_{i+j+k=4} D_{i,j,k} g_x^i g_y^j g_z^k \quad (1)$$

where (g_x, g_y, g_z) are the components of the unit vector \mathbf{g} and the $D_{i,j,k}$'s are the coefficients of the T4 tensor. Such a model may be used to represent ODFs (T4 ODF model). The coefficients are found by minimizing a quadratic cost function under constraints that imposes also the positivity constraint to the estimated tensor model (see (Weldeslassie et al., 2012) for details, see Fig. 1 for a T2–T4 comparison).

2.2 Data Normalization

DW-MRI data sets have to be normalized in a common reference space. Such a spatial normalization is particularly cumbersome for diffusion data, since care must be taken of the underlying fibers.

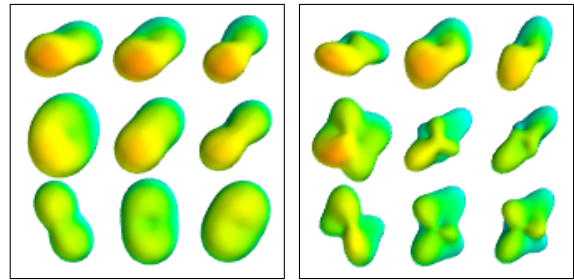


Figure 1: ODF profiles for a given brain area. T2 model (left), T4 model (right). As expected, the T4 model captures more detail and variability than the T2 model.

Considering a T2 model, we compute Fractional Anisotropy (FA) maps which are used to determine a nonlinear transformation between the source and the template data. The estimated transformation is applied on the raw data. The mapped raw data are then reoriented using the local rotation component extracted from the transformation. This amounts to reorientation of the underlying fibers (see (Tao and Miller, 2006; Duarte-Carvajalino et al., 2013)). In practice, we used the patch proposed in (Duarte-Carvajalino et al., 2013), and available in the FSL toolkit (Jenkinson et al., 2012).

2.3 T4 Parameter Space Metric

We have to define a metric in \mathbb{R}^{15} , the T4 parameter space. An Euclidean distance would not be convenient, since it would not take into consideration the specificity of the corresponding underlying ODF.

A point in \mathbb{R}^{15} corresponds to an ODF on the unit sphere. The metric in \mathbb{R}^{15} should thus correspond to a distance between two positive valued functions on the unit sphere. Such a positivity constraint has led to log-based distances (see *e.g.* (Tarantola, 2005)), as is for example the case in the Kullback-Leibler divergence or in the T2 log-Euclidean framework (Arsigny et al., 2006).

Following (Tarantola, 2005), we define the distance between two ODFs d_1 and d_2 as:

$$\mathcal{D}(d_1, d_2) = \int \int \left| \log \frac{d_1(\theta, \phi)}{d_2(\theta, \phi)} \right| \sin \theta \, d\theta \, d\phi \quad (2)$$

where θ and ϕ are the angular parameters on the sphere. This distance induces a metric in \mathbb{R}^{15} , with d_1 and d_2 issued from two points in \mathbb{R}^{15} . This distance is original in the DW-MRI context, to the best of our knowledge. Other (*i.e.* non log-based) distances have been proposed for T4s (see *e.g.* (Barmputis et al., 2007; Du et al., 2014)).

The computation is achieved by discretization in θ and ϕ of the equation above. In practice, a T4 ODF profile d_i is a regression model of noisy data. Moreover, the underlying non noisy data are not necessarily perfectly adequate with a genuine T4 profile. Thereby, the precision in the T4 parameters and in the corresponding ODF profile is not infinite. In addition, a small variation on low ODF values may have a tremendous impact on \mathcal{D} , because of a huge variation of the logarithm. To avoid this harmful effect, we estimate the confidence we have on ODF values by way of a Monte Carlo study, thus yielding a standard deviation error for the ODF. This standard deviation is determined off-line once for all, and each ODF value at stake in the computation of \mathcal{D} by a discrete sum is corrected by addition of the standard deviation.

2.4 ODF Patches

In practice, it is hazardous to rely on the distance \mathcal{D} between two voxels, in particular because of potential registration errors. This is why we resort to a distance based on $3 \times 3 \times 3$ voxel patches. The distance between two patches is defined as the sum of the $3 \times 3 \times 3$ distances between the enclosed couples of ODF profiles. Moreover, the matching patches will be searched among all couples of patches in two $5 \times 5 \times 5$ neighborhoods (one neighborhood for each dataset). Another (popular) option would have been to resort to some kind of data smoothing. We wanted to avoid such a preprocessing, to avoid losing potential important information. Still another option would have been to concentrate on skeletons of white matter fiber bundles (Smith et al., 2006), but still at the expense of losing information.

2.5 Dimension Reduction

We now have a matrix of interpoint distances attached to a voxel of interest (*i.e.* to a $5 \times 5 \times 5$ ROI). Relying on T4s, the underlying space would be \mathbb{R}^s , with $s = 15$ for a mere voxel (no patch), or $s = 3 \times 3 \times 3 \times 15 = 405$ for a 27-voxel patch. Given the number of data points (in the order of 100) in usual studies, the space is sparsely filled. Reducing the dimension will provide more robust and reliable results.

We tested several nonlinear dimension reduction methods, among which Isomap (Tenenbaum et al., 2000), maximum variance unfolding (Weinberger and Saul, 2006), and locality preserving projection (He and Niyogi, 2003; He et al., 2005). There was no significant difference between the aforementioned methods, from a discrimination point of view. We finally chose Isomap, which enables to reproduce the initial

structure of points in a reduced space, say \mathbb{R}^2 or \mathbb{R}^3 , by preserving the geodesic interpoint distances. Scree plots lead us to work in \mathbb{R}^2 , as is the case in (Verma et al., 2007).

2.6 Statistical Reduced Space Model

Each of the two populations (normal and abnormal) corresponds to a set of points in the reduced space. We represent the probability densities p_1 and p_2 corresponding to the populations using kernel density estimation, with a Gaussian kernel (Hastie et al., 2011). One Gaussian kernel is attached to each point. There is one parameter to be determined for each population, which is the covariance matrix attached to each point of this population. These matrices are determined using Scott's rule (Scott, 1992).

The discrepancy between densities p_1 and p_2 has to be quantified. The Kullback-Leibler divergence and its symmetrized version are popular choices. Nevertheless, in the case of a mixture of Gaussian distributions corresponding to our kernel density estimation, there is no closed formula available and the numerical estimation of the Kullback-Leibler divergence is time consuming. We rely on another discrepancy measure, noted \mathcal{P} , which provides good results with a low computation time (Sfikas et al., 2005). The computation of \mathcal{P} is about 150 times faster than the computation of the symmetrical Kullback-Leibler distance in the present case. The discrepancy \mathcal{P} writes:

$$\mathcal{P}(p_1, p_2) = -\log \left[\frac{2 \int p_1(\mathbf{x}) p_2(\mathbf{x}) d\mathbf{x}}{\int (p_1(\mathbf{x}))^2 d\mathbf{x} + \int (p_2(\mathbf{x}))^2 d\mathbf{x}} \right] \quad (3)$$

Considering the mixtures

$$\begin{cases} p_a(\mathbf{x}) &= \sum_{i=1}^I \pi_i^{(a)} \mathcal{N}(\mathbf{x}; \boldsymbol{\mu}_i^{(a)}, \boldsymbol{\Sigma}_i^{(a)}) \\ p_b(\mathbf{x}) &= \sum_{j=1}^J \pi_j^{(b)} \mathcal{N}(\mathbf{x}; \boldsymbol{\mu}_j^{(b)}, \boldsymbol{\Sigma}_j^{(b)}) \end{cases} \quad (4)$$

a straightforward computation yields

$$\int p_a(\mathbf{x}) p_b(\mathbf{x}) d\mathbf{x} = \sum_{i,j} \pi_i^{(a)} \pi_j^{(b)} \sqrt{\frac{\exp(k) |\mathbf{V}|}{(2\pi)^{N_x} |\boldsymbol{\Sigma}_i^{(a)}| |\boldsymbol{\Sigma}_j^{(b)}|}} \quad (5)$$

where N_x is the dimension of \mathbf{x} and with

$$\mathbf{V} = \left(\left(\boldsymbol{\Sigma}_i^{(a)} \right)^{-1} + \left(\boldsymbol{\Sigma}_j^{(b)} \right)^{-1} \right)^{-1} \quad (6)$$

$$k = \boldsymbol{\mu}^T \mathbf{V}^{-1} \boldsymbol{\mu} - \boldsymbol{\mu}_i^{(a)T} \left(\boldsymbol{\Sigma}_i^{(a)} \right)^{-1} \boldsymbol{\mu}_i^{(a)} - \boldsymbol{\mu}_j^{(b)T} \left(\boldsymbol{\Sigma}_j^{(b)} \right)^{-1} \boldsymbol{\mu}_j^{(b)} \quad (7)$$

$$\boldsymbol{\mu} = \mathbf{V} \left(\left(\boldsymbol{\Sigma}_i^{(a)} \right)^{-1} \boldsymbol{\mu}_i^{(a)} + \left(\boldsymbol{\Sigma}_j^{(b)} \right)^{-1} \boldsymbol{\mu}_j^{(b)} \right) \quad (8)$$

and from which we derive $\mathcal{P}(p_1, p_2)$ (we pick a in $\{1, 2\}$ and b in $\{1, 2\}$). Indices i, j, a, b have been dropped from \mathbf{V} , k , and $\boldsymbol{\mu}$ for the sake of simplicity. The preceding formulas may be simplified, since $\boldsymbol{\Sigma}_i^{(a)}$ does not depend on i and since $\boldsymbol{\Sigma}_j^{(b)}$ does not depend on j .

The discrepancy \mathcal{P} is a statistic. We have to estimate the corresponding p-value v^* , *i.e.* the probability of getting a distance \mathcal{P} larger than the reference one $\mathcal{P}(p_1, p_2)$ under the hypothesis that both populations are indiscernible. This will be achieved resorting to permutation testing. Besides, we want to determine a confidence interval associated to the estimation of v^* . This interval will depend on the number of permutations (*i.e.* label shufflings) used. To address these issues, we will resort to the Bayesian framework.

We shuffle N times the labels of the points in the reduced space, and for each shuffling we compute the value of \mathcal{P} . Comparison of the n^{th} sample of \mathcal{P} with the reference $\mathcal{P}(p_1, p_2)$ yields a binary value q_n , which is a sample of the Bernoulli distribution of (unknown) parameter v^* . The problem is now the estimation of v^* from binary samples q_1, \dots, q_N . Using a uniform prior for v , we derive the posterior $p(v|q_1, \dots, q_N)$. The confidence interval (or credibility interval) in v is taken here as being the smallest interval capturing 99 % of the *a posteriori* mass, which is known as Highest Probability Density (HPD) interval in the Bayesian framework. We thus obtain a confidence interval for the p-value. If needed, the length of the confidence interval may be reduced by using more shufflings.

Finally, the voxels are sorted according to increasing p-values. The most dissimilar voxels (the biomarkers) appear on top of the list. We do not address multiple comparison issues here, since we do not provide a list of voxels considered as significantly different between populations. This is left for future work.

3 EXPERIMENTAL RESULTS

In this section, we present experimental results based on synthetic data and on real data. The pathology of

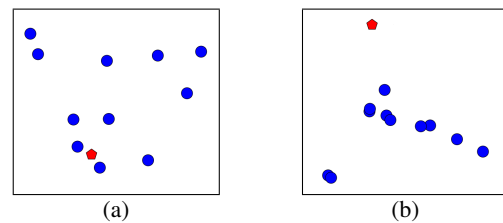


Figure 2: Reduced space for (a) an Euclidean distance and (b) the proposed distance in presence of an outlier (red point). The outlier is well isolated in (b), as should be the case.

interest for real data is *Neuromyelitis Optica* (NMO) (see *e.g.* http://en.wikipedia.org/wiki/Neuromyelitis_optica).

3.1 Material

The proposed statistical model was implemented in Python. The FSL toolbox (Jenkinson et al., 2012) was used for the registration step.

Synthetic data were generated using a code written by A. Barmpoutis *et al.* (Barmpoutis et al., 2009).

Real data are composed of 22 normal (control) and 36 abnormal DW-MRI datasets. Brain acquisition consisted in High Angular Resolution Diffusion Imaging (HARDI) with 30 non colinear directions of gradients. The size of the images is $128 \times 128 \times 41$ for a resolution of $1.8 \times 1.8 \times 3.5 \text{ mm}^3$. The b-value is equal to 1000 s/mm^2 .

3.2 Results

Influence of the metric. In Fig. 2, we compare two reduced spaces obtained respectively with an Euclidean distance (L_2 norm) and with the proposed distance, both on the ODF profiles and for T4 parameterization. The outlier is an ODF resulting from a tensor for which one coefficient was divided by a factor 60. As expected, this outlier is separated from the rest of the group in the case of the proposed metric, but not in the case of the Euclidean metric.

Reduced space model and statistical test. We represent the reduced space for three voxels in Fig. 3. The corresponding p-value HPD intervals are reported in Table 1. The first voxel is typical of a dissimilar configuration for both populations, whereas the second and third voxels are typical of similar configurations for both populations.

The first voxel examined indicates that the two ODF populations are different (see Fig. 3, case (a)). If we resort to smoothing instead of using patches, the populations do not differ anymore according to this voxel. Information has been lost in the smoothing, thus hampering the diagnosis potential.

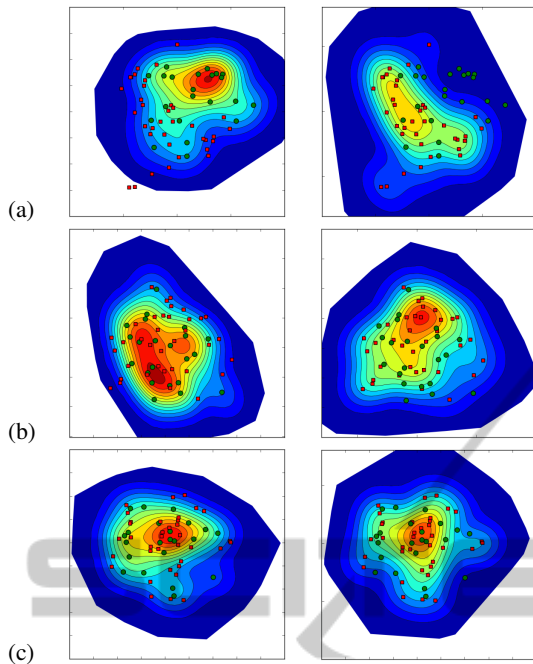


Figure 3: Representation of probability densities in the reduced space. Green dots: normal cases; red squares: abnormal cases. (a) dissimilar populations; (b) and (c) similar populations. Left column: representation of the probability density corresponding to the normal population; right column: representation of the probability density corresponding to the abnormal population (blue: low density; red: high density. The same color scale is used across all subfigures.). The densities correspond to kernel density estimation with a Gaussian kernel.

Table 1: P-value HPD intervals of the cases depicted in Fig. 3. We used 1000 shuffles. It took approximately 3 minutes on a standard computer to process each voxel. Most of the computation time was devoted to determining the patch correspondence.

Fig.3 Cases	p-value HPD interval	width of interval	Decision
(a)	[0, 0.0046]	0.0046	Dissimilar
(b)	[0.35, 0.43]	0.08	Similar
(c)	[0.988, 0.999]	0.011	Similar

T2-T4 comparison on Synthetic Data. We consider a case of two fibers crossing at 90 degrees. Both fibers have the same amplitude. The two populations differ by a rotation angle of 5 degrees affecting both fibers likewise. Noise was added to the synthetic data. The T4 model is able to discriminate the two populations, whereas the T2 model is not able to do so (this fiber crossing is seen by the T2 model as an isotropic ODF, independently of the rotation angle).

Comparison of the proposed Statistical Test with the Hotelling Test on Synthetic Data. We consider a

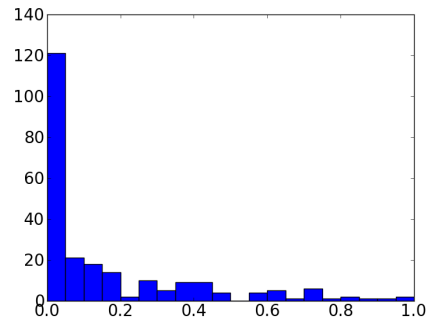


Figure 4: Distribution of p-values for a NMO-related ROI. As expected, a large number of voxels have low p-values and are thus identified as abnormal.

case of crossing fibers, where the angle between the two fibers differs from one population to the other (the values considered are 90 degrees for the normal population, and 85 degrees for the abnormal population). The amplitude of the fibers are different as well (the amplitude is 1 for the fiber common to both populations; for the fiber with a different orientation in both populations, the amplitude is 0.35 for the normal population, and 0.45 for the abnormal population).

The proposed statistical test is able to discriminate both populations. Besides, we perform a Hotelling test. This test takes place in the reduced space. Each population is modeled by a Gaussian distribution, and means are compared, looking for a statistical difference. The Hotelling test was not able to discriminate both populations.

T2-T4 comparison on Real Data. We compared the results (similar/dissimilar) issued from T2 model and from T4 model. Whenever the results disagreed, it happened that the T4 model gave the correct answer and that the T2 model was not able to capture all information conveyed by the data. This was validated by testing the residuals (the dissimilarity information is contained in the T2 residual). Using a log-Euclidean distance on second order tensors to reduce the dimension of the data yields globally the same results as those issued by the metric we propose, when applied on T2 profiles.

P-value Distribution on Real Data. On Fig. 4, we represent the distribution of p-values (one p-value for each voxel), for a region of interest (ROI). The ROI is identified as being sensitive to the disease of interest (NMO). This is confirmed on the plot, where a peak of low p-values appears.

The proposed statistical T4 model is robust and sensitive. On the evaluation tests proposed, it showed better performance than models relying on Euclidean (L_2) norms or on T2 ODF profiles. The proposed model is thus pertinent to extract biomarkers with a view to early diagnosis in NMO. Other pathologies

are concerned as well.

4 CONCLUSION

We proposed an original statistical model for fourth order tensor ODF modeling of DW-MRI. This model incorporates a suitable metric in the parameter space. It relies on nonlinear dimension reduction, and on an original statistic in the reduced space, allowing to compare two populations and to extract biomarkers. This approach has shown better ability to discriminate two populations, as compared to models relying on other metrics, on T2 ODF profiles, or on the Hotelling test. It has thus a potential for early diagnosis.

Resorting to T4 ODF profiles will also enable us to identify more precisely the changes effectively taking place between the two populations, as compared to changes identified by T2 models where the profiles are described less accurately. This is left for future work.

REFERENCES

- Arsigny, V., Fillard, P., Pennec, X., and Ayache, N. (2006). Log-Euclidean metrics for fast and simple calculus on diffusion tensors. *Magnetic Resonance in Medicine*, 56(2):411–421.
- Barmpoutis, A., Bing, J., and Vemuri, B. (2009). Adaptive kernels for multi-fiber reconstruction. In *Proceedings of the Information Processing in Medical Imaging conference (IPMI)*, volume 21, pages 338–349.
- Barmpoutis, A., Vemuri, B., and Forder, J. (2007). Registration of high angular resolution diffusion MRI images using 4th order tensors. In *Int. Conf. on Medical Image Computing and Computer Assisted Intervention (MICCAI)*, volume 4791 of *Lecture Notes in Computer Science*, pages 908–915. Springer.
- Du, J., Goh, A., Kushnarev, S., and Qiu, A. (2014). Geodesic regression on orientation distribution functions with its application to an aging study. *NeuroImage*, 87:416–426.
- Duarte-Carvajalino, J., Sapiro, G., Harel, N., and Lenglet, C. (2013). A framework for linear and non-linear registration of diffusion-weighted MRIs using angular interpolation. *Frontiers in Neuroscience*, 7.
- Hastie, T., Tibshirani, R., and Friedman, J. (2011). *The elements of statistical learning*. Springer, second edition.
- He, X. and Niyogi, P. (2003). Locality preserving projections. In *Advances in Neural Information Processing Systems 16 (NIPS)*, volume 16, pages 153–160.
- He, X., Yan, S., Hu, Y., Niyogi, P., and Zhang, H.-J. (2005). Face recognition using Laplacianfaces. *IEEE Transactions on Pattern Analysis and Machine Intelligence*, 27(3):328–340.
- Horsfield, M. A. and Jones, D. K. (2002). Applications of diffusion-weighted and diffusion tensor MRI to white matter diseases – a review. *NMR in Biomedicine*, 15(7-8):570–577.
- Jenkinson, M., Beckmann, C., Behrens, T., Woolrich, M., and Smith, S. (2012). FSL. *NeuroImage*, 62(2):782–790.
- Jones, D. K. (2011). *Diffusion MRI: theory, methods, and applications*. Oxford University Press.
- Ozarslan, E. and Mareci, T. H. (2003). Generalized diffusion tensor imaging and analytical relationships between diffusion tensor imaging and high angular resolution diffusion imaging. *Magnetic Resonance in Medicine*, 50(5):955–965.
- Scott, D. (1992). *Multivariate density estimation: theory, practice, and visualization*. Wiley.
- Sikas, G., Constantinopoulos, C., Likas, A., and Galatsanos, N. (2005). An analytic distance metric for Gaussian mixture models with application in image retrieval. In *15th International Conference on Artificial Neural Networks (IEEE ICANN 2005)*, volume 3697 of *Lecture Notes in Computer Science*, pages 835–840. Springer.
- Smith, S., Jenkinson, M., Johansen-Berg, H., Rueckert, D., Nichols, T., Mackay, C., Watkins, K., Ciccarelli, O., Cader, M. Z., Matthews, P., and Behrens, T. (2006). Tract-based spatial statistics: voxelwise analysis of multi-subject diffusion data. *NeuroImage*, 31(4):1487–1505.
- Tao, X. and Miller, J. (2006). A method for registering diffusion weighted magnetic resonance images. In *Int. Conf. on Medical Image Computing and Computer Assisted Intervention (MICCAI)*, volume 4191 of *Lecture Notes in Computer Science*, pages 594–602. Springer.
- Tarantola, A. (2005). *Elements for physics: quantities, qualities, and intrinsic theories*. Springer.
- Tenenbaum, J. B., Silva, V., and Langford, J. C. (2000). A global geometric framework for nonlinear dimensionality reduction. *Science*, 290(5500):2319–2323.
- Tuch, D. S. (2004). Q-ball imaging. *Magnetic Resonance in Medicine*, 52(6):1358–1372.
- Verma, R., Khurd, P., and Davatzikos, C. (2007). On analyzing diffusion tensor images by identifying manifold structure using isomaps. *IEEE Transactions on Medical Imaging*, 26(6):772–778.
- Weinberger, K. and Saul, L. (2006). Unsupervised learning of image manifolds by semidefinite programming. *International Journal of Computer Vision*, 70(1):77–90.
- Weldeselassie, Y., Barmpoutis, A., and Atkins, M. (2012). Symmetric positive-definite Cartesian tensor fiber orientation distribution (CT-FOD). *Medical Image Analysis*, 16(6):1121–1129.